

Cleavage of model substrates by archaeal RNase P: role of protein cofactors in cleavage-site selection

Sylvie Sinapah¹, Shiyong Wu¹, Yu Chen¹, B. M. Fredrik Pettersson¹, Venkat Gopalan² and Leif A. Kirsebom^{1,*}

¹Department of Cell and Molecular Biology, Biomedical Centre, Uppsala University SE-751 24, Uppsala, Sweden and ²Department of Biochemistry, Center for RNA Biology, The Ohio State University, Columbus, OH 43210, USA

Received September 7, 2009; Revised July 30, 2010; Accepted August 2, 2010

ABSTRACT

RNase P is a catalytic ribonucleoprotein primarily involved in tRNA biogenesis. Archaeal RNase P comprises a catalytic RNase P RNA (RPR) and at least four protein cofactors (RPPs), which function as two binary complexes (POP5•RPP30 and RPP21•RPP29). Exploiting the ability to assemble a functional *Pyrococcus furiosus* (*Pfu*) RNase P *in vitro*, we examined the role of RPPs in influencing substrate recognition by the RPR. We first demonstrate that *Pfu* RPR, like its bacterial and eukaryal counterparts, cleaves model hairpin loop substrates albeit at rates 90- to 200-fold lower when compared with cleavage by bacterial RPR, highlighting the functionally comparable catalytic cores in bacterial and archaeal RPRs. By investigating cleavage-site selection exhibited by *Pfu* RPR (±RPPs) with various model substrates missing consensus-recognition elements, we determined substrate features whose recognition is facilitated by either POP5•RPP30 or RPP21•RPP29 (directly or indirectly via the RPR). Our results also revealed that *Pfu* RPR + RPP21•RPP29 displays substrate-recognition properties coinciding with those of the bacterial RPR-alone reaction rather than the *Pfu* RPR, and that this behaviour is attributable to structural differences in the substrate-specificity domains of bacterial and archaeal RPRs. Moreover, our data reveal a hierarchy in recognition elements that dictates cleavage-site selection by archaeal RNase P.

INTRODUCTION

The ubiquitous endoribonuclease RNase P is responsible for generating matured tRNAs with monophosphate at

their 5'-end. In Bacteria, the holoenzyme consists of one RNA (RPR) and one protein (RPP) subunit while in Archaea and Eukarya the number of proteins are at least four and nine, respectively (1–3). Irrespective of the source, the RNA is the catalytic subunit of RNase P and it can mediate cleavage at the correct position in the absence of protein (4–9). An interesting variant is the recently reported RNase P-like activity derived from human mitochondria that consists of a complex of three proteins (10).

Lowered metal ion requirement and increased efficiency of cleavage by the holoenzyme compared with the RPR-alone reaction is attributable to the bacterial RPP enhancing the RPR's affinity for the precursor tRNA (ptRNA) and catalytically important metal ions, accelerating product release from the RPR and preventing rebinding of the 5'-matured tRNA cleavage product to the RPR; the bacterial RPP also broadens substrate specificity and stabilizes the native structure of the RPR (11–22). In contrast to these detailed insights on the bacterial RPP, little is known about the role and function of the various RPPs in archaeal and eukaryal RNase P, although there are reasons to expect contributions from archaeal/eukaryal RPPs in this regard. For example, the multi-protein human RNase P holoenzyme differs from the human RPR in that it does not cleave model hairpin stem-loop substrates, although the caveat remains that assay conditions used were different in the two cases (7,23). Moreover, cleavage of the atypical precursor tRNA^{His} by the eukaryotic RNase P holoenzyme generates a mature tRNA with a 7-bp-long acceptor stem (3,24–26); in contrast, human RPR (without any protein subunits) cleaves precursor tRNA^{His} at the same position as bacterial RPR resulting in an 8-bp long acceptor stem (7). While these studies suggest that RPPs influence cleavage-site selection, the inability to reconstitute eukaryotic RNase P has prevented identification of the RPPs (and the underlying mechanisms) responsible for these substrate-recognition effects.

*To whom correspondence should be addressed. Tel: +46 18 471 4068; Fax: +46 18 53 03 96; Email: leif.kirsebom@icm.uu.se

The authors wish it to be known that, in their opinion, the first three authors should be regarded as joint First Authors.

© The Author(s) 2010. Published by Oxford University Press.

This is an Open Access article distributed under the terms of the Creative Commons Attribution Non-Commercial License (<http://creativecommons.org/licenses/by-nc/2.5>), which permits unrestricted non-commercial use, distribution, and reproduction in any medium, provided the original work is properly cited.

As a model for the biochemically intractable eukaryotic counterpart, we have used *Pyrococcus furiosus* (*Pfu*) RNase P in our substrate-recognition studies. Archaeal RNase P presents an interesting montage made up of an RNA, which bears striking resemblance to the bacterial counterpart, and four proteins, which have eukaryotic homologs. Such a mosaic ribonucleoprotein (RNP) offers an opportunity to dissect subtle and complex inter-subunit functional cooperation, which likely resulted from dynamic co-evolution of RNPs. Our work plan was also motivated by the ability to reconstitute *Pfu* RNase P from *in vitro* transcribed RPR and four recombinant RPPs (6).

Apart from ptRNAs, several other RNAs have been demonstrated to be RNase P substrates [Kirsebom (2007) and references therein]. For example, short model hairpin loop substrates are cleaved both by bacterial and eukaryal RPRs (7,27). Recently, we examined cleavage of model substrates by bacterial RPR and provided experimental evidence for an induced fit that is mediated by an interaction between the T-stem/loop (TSL-region) and the RPR's TSL-binding-site (TBS-region) (28). On the basis of these findings, we decided to investigate whether archaeal RPRs could cleave model substrates, especially since their TBS-region differs from that in bacterial RPRs [e.g. *Escherichia coli* RNase P RNA, M1 RNA or *Eco* RPR; (29)], and archaeal RPPs influenced cleavage-site selection. Here we present data demonstrating that *Pfu* RPR can cleave model hairpin loop substrates, some comprising only 3 bp. Moreover, by using substrates lacking specific structural elements and mapping the cleavage-site selection exhibited by the archaeal RPR in the absence and presence of the full or partial suite of RPPs, we have gained insights into how protein cofactors influence the substrate-recognition properties of their cognate RNA catalyst.

MATERIALS AND METHODS

Preparation of substrates, *Eco* and *Pfu* RPRs, RPP21•RPP29 and POP5•RPP30

The different substrate variants of pATSer and pMini3bp were purchased from Dharmacon, USA and labelled with ³²P at the 5'-end with [γ -³²P]ATP as previously described (28).

The *Eco* (M1 RNA) and *Pfu* RPR variants were generated as T7 RNA polymerase run-off transcripts as described in detail elsewhere [(30) and references therein]. The *Pfu* RPR variant RPR_{C270} behind the T7 promoter was generated using QuikChange Site-Directed Mutagenesis (Stratagene) with appropriate oligonucleotides and the plasmid pBT7-*Pfu* RPR (6) as template. The archaeal-bacterial chimeric RPR_{ECS3} derivative was generated using PCR as described in Supplementary information.

Pfu RPPs (RPP21, RPP29, RPP30 and POP5) were purified and used as described elsewhere [(6); Chen *et al.*, in press).

RNase P assays

RNA-alone reactions. Cleavage was conducted in buffer C [50 mM MES (pH 6.1 at 37°C), 0.8 M NH₄OAc and specified Mg(OAc)₂ concentrations and temperature]. The assay pH was chosen on the basis of previous reports suggesting that cleavage is rate limiting at pH 6.1 for *Eco* RPR-mediated catalysis [(31) and references therein]. For the Mg²⁺ titration and cleavage-site recognition experiments, the final concentrations of *Eco* and *Pfu* RPRs were between 1.6 and 3.7 μM as indicated while the substrate concentration was ~0.02 μM (for all substrates tested). Prior to initiating the reaction, the substrate and RPR were pre-incubated at the indicated temperature for 2 and 10 min, respectively. The longer pre-incubation time for RPR ensures optimal folding of the RNA (6,30).

Determining if cleavage of the enzyme-substrate (ES) complex is slower than its dissociation (ref 32 and references therein). Pre-folded *Pfu* RPR (3.7 μM) was mixed together with ~0.02 μM substrate in 20 μl and incubated at 37°C. Ten minutes after the initiation of the reaction, 10 μl from this mixture was transferred to 2 ml of dilution buffer C containing 800 mM Mg(OAc)₂. At each time point post dilution, a 200-μl aliquot was removed and reaction contents precipitated by adding 700 μl of 99.5% ethanol, 20 μl of 3 M NaOAc (pH 5.1) and 2 μl of glycogen (20 mg/ml). The samples were frozen at -20°C overnight followed by centrifugation for 40 min at ×16000g in a micro-centrifuge (Eppendorf) at 4°C. The precipitated RNA was dried, dissolved in 10 μl of H₂O and 20 μl of stop solution [10 M urea, 10 mM EDTA, 0.025% (w/v) bromophenol blue and 0.025% (w/v) xylene cyanol] and the reaction products were analyzed as described below. (Note: In parallel, a control experiment was conducted with 3.7 μM *Pfu* RPR and ~0.02 μM substrate, wherein substrate cleavage was followed as a function of time in the absence of dilution after 10 min.)

Cleavage in the presence of *Pfu* RPP21•RPP29 and POP5•RPP30. Formation of partially or fully reconstituted *Pfu* RNase P holoenzymes with RPP21•RPP29, POP5•RPP30 or both binary RPP complexes were performed essentially as described elsewhere (6). The reactions were performed in a final volume of 10 μl in buffer D [50 mM Tris-HCl (pH 7.5), 800 mM NH₄OAc and 30 mM (or 300 mM) MgCl₂]. While the final concentration of *Pfu* RPR was 0.5 μM for the RPR-alone reaction, it was 0.25, 0.05 and 0.01 μM in the presence of RPP21•RPP29, POP5•RPP30 and all four RPPs, respectively. The RPPs were typically used at a concentration that was 5- to 10-fold greater than that of the RPR. RNP assembly was performed as follows. Briefly, *Pfu* RPR was incubated in DEPC-treated H₂O for 50 min at 50°C. This was followed by incubation at 37°C for 30 min. Then, buffer D and MgCl₂ were added to give the final concentrations stated above in the final reaction mixture and followed by incubation for 10 min at 37°C. After these pre-incubations, the different RPPs were added and

incubations continued first for 5 min at 37°C and then for 10 min at 55°C. The processing reactions at 55°C were initiated by the addition of 2 μ l of [γ -³²P]-labelled substrate. Both the RPR-alone and RPR + RPP reactions were terminated at the indicated times by adding two volumes of $\times 1.5$ phenol stop solution [8.4 M urea, 1.2 mM EDTA, 0.036% (w/v) bromophenol blue, 0.036% (w/v) xylene cyanol and 20% (v/v) phenol]. The cleavage products were analyzed as described below.

Analysis of cleavage products. Products generated by RNase P (and re-suspended in the appropriate stop dyes) were separated by electrophoresis on denaturing 22% (w/v) polyacrylamide gels [10 mM Tris-borate (pH 7.5), 1 mM EDTA and 7 M urea], detected with a Phosphoimager (Molecular Dynamics 400S) and the signals were quantitated using the software ImageQuant (Molecular Dynamics).

Determination of the kinetic constants k_{obs} and $k_{\text{obs}}/K^{\text{sto}}$, and Hill coefficients

The kinetic constants k_{obs} and $k_{\text{obs}}/K^{\text{sto}}$ were determined under saturating single turnover conditions in buffer C containing 800 mM Mg(OAc)₂ (saturating Mg²⁺ concentration for cleavage by *Pfu* RPR alone; Figure 3) as described elsewhere [(28) and references therein]. The final concentration of substrates (pATSerUG and pMini3bpUG) was $\leq 0.02 \mu\text{M}$ while the concentration of the RPR ranged between 0.4 μM and 30 μM , depending on the RPR and substrate being tested. For rate calculations, the incubation times (at 37°C or 55°C) for each substrate were adjusted to ensure that velocity measurements were in the linear range. The values for k_{obs} and $k_{\text{obs}}/K^{\text{sto}}$ were obtained by linear regression analysis of Eadie-Hofstee plots.

The Hill coefficients (n) for cleavage of pATSerUG and pMini3bpUG were determined from the slopes of plots of $\log[v/(V_{\text{max}} - v)]$ versus $\log[\text{Mg}^{2+}]$ [see (33) and references therein].

RESULTS

Cleavage of a hairpin loop substrate by *Pfu* RPR

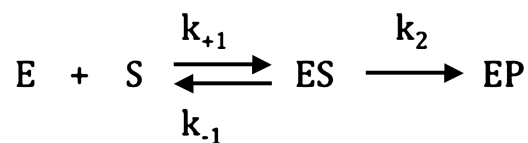
Cleavage of the model hairpin loop substrate pATSerUG (Figure 1) by *Eco* RPR has been used extensively in our studies of bacterial RPR (7,28,31,34–40). Hence, we chose pATSerUG to investigate whether *Pfu* RPR could cleave model hairpin loop substrates, and extended these studies to include model hairpin substrates with only 3- or 4-bp stems capped by a GAAA-tetra loop. The latter substrates are referred to as pMini3bpUG and pMini3bpCG, respectively [Figure 1; (28)]. First, we studied cleavage at either 37°C or 55°C and as a function of Mg²⁺ under single turnover conditions at pH 6.1; in the case of pMini3bpUG, experiments were only performed at 37°C. The higher temperature of 55°C was chosen since *Pfu* is a hyperthermophile, while studies at 37°C allowed us to compare the *Pfu* RPR results with previous findings on the bacterial RPR [(6,28) and references therein]. Below, cleavage at +1 refers to phosphodiester hydrolysis between –1 (the last nucleotide of the 5'-leader) and +1

(the first nucleotide of the 5'-matured product), and miscleavage refers to bond breakage between –2 (the penultimate nucleotide of the 5'-leader) and –1.

As inferred from the mobility of the 5'-cleavage fragments, *Pfu* RPR (like *Eco* RPR) cleaved pATSerUG at +1 (Figure 2 lanes 4 and 7). Maximum cleavage by *Pfu* RPR required a high concentration of Mg²⁺, with activity plateauing at ~ 600 mM, irrespective of temperature (Figure 3; data not shown). This Mg²⁺ requirement is significantly higher compared with cleavage of the same substrate by *Eco* RPR wherein maximal activity is observed at ~ 200 mM (28). *Pfu* RPR also cleaved pMini3bpUG at +1. Interestingly, similar Mg²⁺ profiles were observed for both pATSerUG and pMini3bpUG (Figure 3). This observation contrasts with *Eco* RPR, which requires ~ 200 and ~ 600 mM Mg²⁺ for optimal cleavage of pATSerUG and pMini3bpUG, respectively [(28), Wu and Kirsebom, unpublished data].

From Figure 3, we also calculated the Hill coefficients for cleavage of pATSerUG to be 4.2 and 4, respectively. These values are similar to those reported for bacterial RNase P (20) and are consistent with a minimal requirement of four Mg²⁺-binding sites to stabilize the *Pfu* RPR-pATSerUG (or –pMini3bpUG) complex, highlighting parallels in cleavage of different substrates, and in the mechanism of action of archaeal and bacterial RPRs. Although the Hill equation permits quantitative comparisons of results from independent investigations on RNase P variants, drawing parallels is complicated by possible differential displacement of ions upon substrate binding and differences in ion-atmosphere effects or ionic strength (dissimilar in different studies).

Next, we determined the kinetic constants k_{obs} and $k_{\text{obs}}/K^{\text{sto}}$ at 37°C and 55°C for cleavage of pATSerUG under saturating single turnover conditions at pH 6.1 and at 800 mM Mg²⁺ (Figure 4). From the simplified Scheme 1



$k_{+1} = k_{\text{obs}}/K^{\text{sto}}$ (which corresponds to $k_{\text{cat}}/K_{\text{m}}$ as determined under multiple turnover conditions) while k_{obs} reflects k_2 , the rate of cleavage. Moreover, to assess whether $K^{\text{sto}} \approx K_{\text{d}}$, which is the case when $k_{-1} \gg k_2$ (32), we performed a pulse-chase experiment under $[\text{E}] \gg [\text{S}]$ conditions (see 'Materials and Methods' section). Our data (Figure 1 in Supplementary Data) showed that through large dilution of a pre-assembled ES-complex, generated with either pATSerUG or pMini3bpUG, the substrate could be dissociated from the enzyme (RPR) preventing any further increase in rate of cleavage post-dilution due to the inability of the substrate to rebind for cleavage. These data are consistent with $k_{-1} \gg k_2$ and $K^{\text{sto}} \approx K_{\text{d}}$ under these reaction conditions.

Comparing k_{obs} for *Pfu* and *Eco* RPR at 37°C revealed that *Pfu* RPR cleaved pATSerUG with a 200-fold slower rate than *Eco* RPR (Table 1). By increasing the temperature to 55°C, the *Pfu* RPR's k_{obs} increased ~ 60 -fold. The

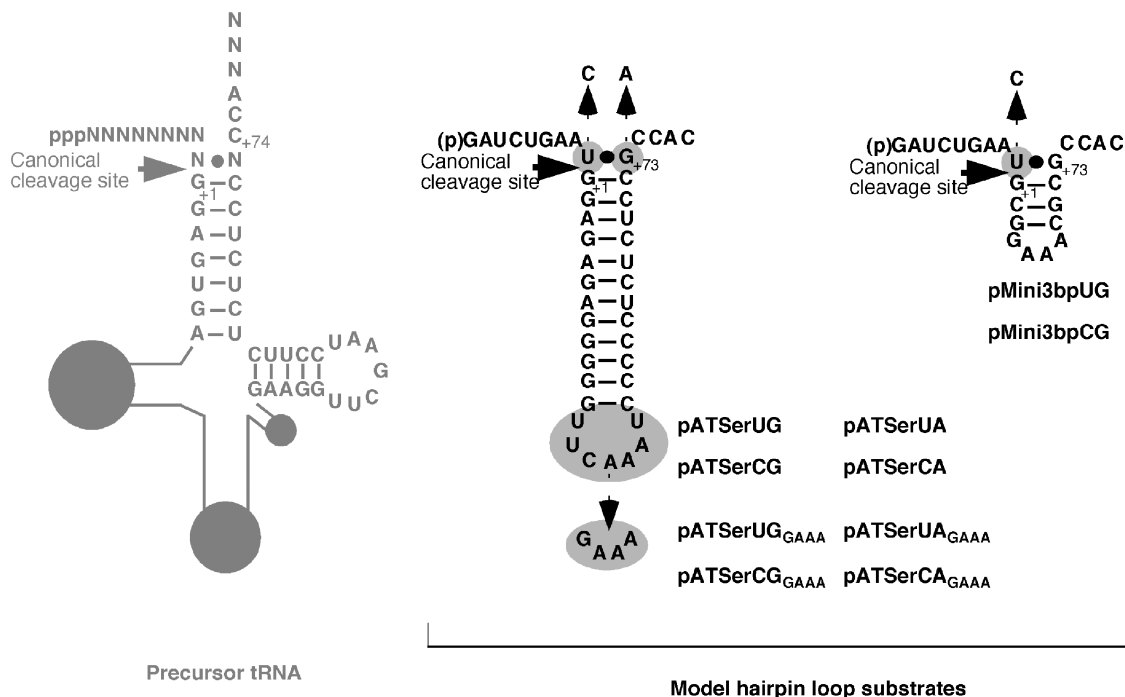


Figure 1. Comparison of the predicted secondary structures of a ptRNA in grey and the model hairpin loop substrates used in this study. The highlighted regions/residues in the model substrates, pATSer and pMini3bp, were substituted to generate the different variants as indicated. The canonical RNase P cleavage sites between residues -1 and $+1$ are marked with arrows. The residue numbering of the residues near the cleavage site follows that of a ptRNA (e.g. the residue immediately preceding the 3'-terminal CCA-motif corresponds to the discriminator base at position $+73$).

Table 1. The kinetic constants k_{obs} and $k_{\text{obs}}/K^{\text{sto}}$ for cleavage of various substrates by *Eco* and *Pfu* RPRs

RPR	Substrate/Assay temp	k_{obs} (min^{-1})	$k_{\text{obs}}/K^{\text{sto}}$ ($\text{min}^{-1} \times \mu\text{M}^{-1}$)	K_{d} (μM)
<i>Eco</i>	pATSerUG 37°C	12 ± 1.3	19 ± 3.8	ND
<i>Pfu</i>	pATSerUG 37°C	0.058 ± 0.006	0.03 ± 0.005	1.9
<i>Pfu</i>	pATSerUG 55°C	3.8 ± 0.5	0.19 ± 0.4	20
<i>Eco</i>	pMini3bpUG 37°C	7.2 ± 2.2	13 ± 8.3	ND
<i>Pfu</i>	pMini3bpUG 37°C	0.08 ± 0.008	0.044 ± 0.01	1.8

The experiments were performed under saturating single-turnover conditions at pH 6.1 and 800 mM Mg^{2+} as described in 'Materials and Methods' section. The final concentration of substrate was ≤ 20 nM. The concentration of the different RPR variants was varied between 0.4 and 30 μM and the concentration range varied depending on the RPR and substrate used. ND, not determined.

k_{obs} and $k_{\text{obs}}/K^{\text{sto}}$ are quite similar for cleavage of pATSerUG and pMini3bpUG by *Pfu* RPR. Additionally, since $K^{\text{sto}} \approx K_{\text{d}}$, we infer that these two substrates bind to *Pfu* RPR with equal affinity. The k_{obs} values reported here are lower compared to cleavage for *Eco* RPR but they are significantly higher than the value previously reported for another archaeal RPR (8); however, this difference is not wholly unexpected given that Li *et al.* (8) determined k_{obs} at a lower Mg^{2+} concentration (100 mM) and lower temperature (37°C),

used a precursor tRNA substrate and a different RPR (from *Methanothermobacter thermoautotrophicus*).

It is instructive to compare the K_{d} and k_{obs} values for *Pfu* RPR-mediated cleavage of pATSerUG at 37°C versus 55°C (Table 1). The K_{d} increased 10-fold when the temperature was increased from 37°C to 55°C, perhaps as a result of fewer productive ES interactions that would be expected from increased motion of the RPR and substrate at 55°C. However, the k_{obs} increased 60-fold, consistent with the expectation that enzymes from thermophilic sources are weaker catalysts at moderate temperatures, an observation already made with a bacterial RPR from *Thermus thermophilus* (41).

Pfu and *Eco* RPRs show differences in cleavage-site selection

Having established that *Pfu* RPR cleaves model hairpin loop substrates, we decided to study cleavage-site recognition properties and compare it with the bacterial *Eco* RPR. Hence, pATSerCG, pATSerCG_{GAAA} and pMini3bpCG (Figure 1) were selected since *Eco* RPR is known to cleave these three substrates at both $+1$ and -1 , although to a variable extent depending on the substrate (28,34). As shown in Figure 2 (and data not shown), *Pfu* RPR cleaved these three substrates mainly at the $+1$ position. With pATSerCG_{GAAA}, this is a notable difference compared with the cleavage pattern for *Eco* RPR, which cleaves this substrate mainly at the -1 position (28).

Comparing the secondary structures of *Pfu* RPR with *Eco* RPR (Figure 5, area highlighted in dark grey) reveals variations in the paired regions P10 and P11, which are

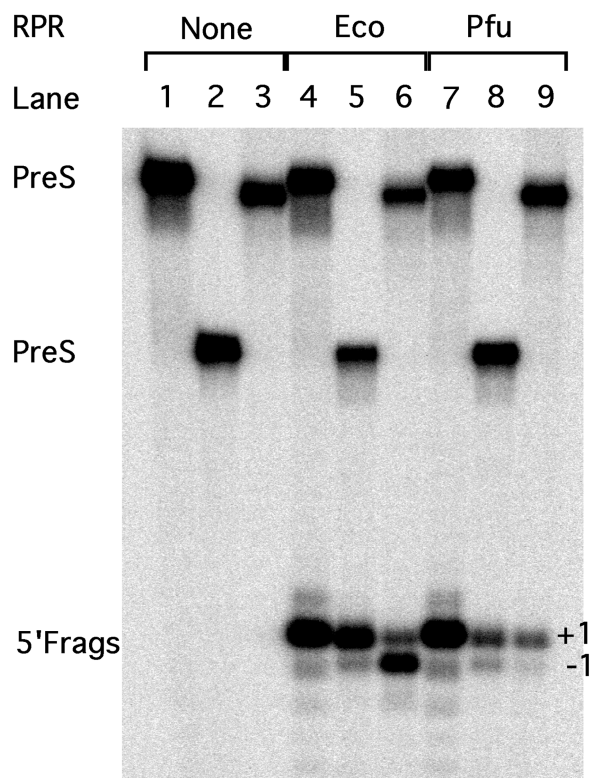


Figure 2. Cleavage of model hairpin loop substrates by *Eco* and *Pfu* RPR as indicated. The reactions were performed at 37°C in buffer C containing 800mM Mg^{2+} . Lane 1, pATSerUG alone; lane 2, pMini3bpCG alone; lane 3, pATSerCG_{GAAA} alone; lane 4, pATSerUG + *Eco* RPR; lane 5, pMini3bpCG + *Eco* RPR; lane 6, pATSerCG_{GAAA} + *Eco* RPR; lane 7, pATSerUG + *Pfu* RPR; lane 8, pMini3bpCG + *Pfu* RPR; and lane 9, pATSerCG_{GAAA} + *Pfu* RPR. Pre, precursor (i.e. pATSerUG, pMini3bpCG and pATSerCG_{GAAA}); 5'-FragS, 5'-cleavage fragments.

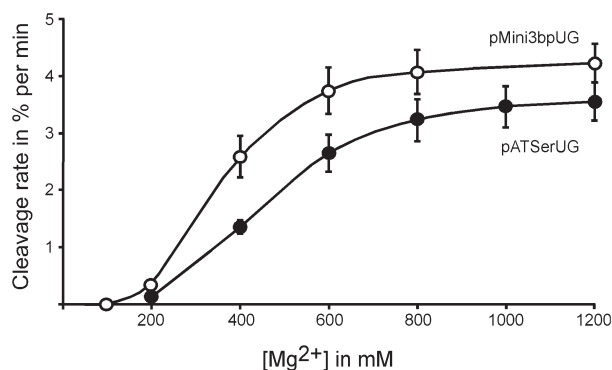


Figure 3. Cleavage of pATSerUG and pMini3bpUG by *Pfu* RPR as a function of Mg^{2+} under single turnover conditions at pH 6.1 (buffer C) and 37°C. The data reported represent an average of at least two independent experiments.

part of the TSL-binding site (TBS) in the S domain. Base substitutions in the *Eco* RPR's TBS suppress the miscleavage of pATSerCG_{GAAA} at -1 (28). Therefore, to examine whether the altered structure of the *Pfu* RPR's TBS in part accounts for its cleavage of pATSerCG_{GAAA} mainly at +1, we replaced the

S domain of *Pfu* RPR with that of *Eco* RPR (Figure 5). This variant is referred to as *Pfu* RPR_{ECS3}. Indeed, *Pfu* RPR_{ECS3} cleaved pATSerCG_{GAAA} with an increased frequency at the -1 position, roughly to the same extent as *Eco* RPR (Figure 6). This suggests that the S domains of *Pfu* and *Eco* RPRs, with their structurally different TBS regions, interact differently with the GAAA-tetra loop in pATSerCG_{GAAA}.

Cleavage of various model hairpin loop substrates in the presence of archaeal RPPs

Model hairpin loop substrates are also cleaved in the presence of RPPs. *Pfu* RNase P consists of an RPR and four RPPs (see above). Cleavage activity can be reconstituted by assembling the RPR with all four proteins or partially with two different binary RPP complexes: RPP21•RPP29 and RPP30•POP5 (6). To investigate whether model hairpin substrates are also cleaved by *Pfu* RPR assembled with these binary RPPs, we tested cleavage of pATSerUG and pMini3bpUG. The assays were performed in the presence of 30 or 300mM Mg^{2+} at 55°C. The RPR with either binary RPP complex or all four RPPs cleaved pATSerUG (Figure 7A, lanes 2–8) as well as the short model substrate pMini3bpUG (Figure 7C, lanes 2–8) at +1. Therefore, *Pfu* RPR can cleave model hairpin loop substrates both with and without cognate RPPs.

Influence of RPP21•RPP29 on cleavage-site recognition. We next assessed the role of *Pfu* RPPs in cleavage-site selection by the catalytic RPR moiety. In the first set of experiments, we focused on the 'TSL/TBS-interaction' (2), which has been suggested to play an important role for efficient cleavage by *Eco* RPR and also account for why the presence of a GAAA-tetraloop (instead of a tRNA T-loop) in pATSerCG_{GAAA} results in its cleavage preferentially at -1 (28). As discussed above, compared to *Eco* RPR (M1 RNA), the secondary structure of the TBS-region in *Pfu* RPR is different from the *Eco* RPR (Figure 5). Taken together with the footprint of RPP21•RPP29 in the archaeal RPR's S domain (42), it is reasonable to expect that this binary complex might influence the TSL/TBS-interaction and/or directly bind to the substrate's TSL region. To address this hypothesis, we focused on pATSerCG_{GAAA}, which is cleaved mainly at the +1 position by *Pfu* RPR (Figure 2; see above).

Indeed, addition of RPP21•RPP29 resulted in substantial cleavage of pATSerCG_{GAAA} at -1 (70%) in striking contrast to POP5•RPP30 (20%) and even the RPR-alone reaction (<6%; Figures 6 and 7E). Addition of all four RPPs also resulted in cleavage preferentially at -1, perhaps indicative of the greater influence of RPP21•RPP29 in the process of selecting the cleavage site in pATSerCG_{GAAA}. Raising the Mg^{2+} concentration to 300mM resulted in a suppression of cleavage at the -1 position with *Pfu* RPR + RPP21•RPP29. Since pATSerCG with an intact T-loop was cleaved mainly at the +1 position both in the absence and in the presence of the RPPs (Figure 7D), miscleavage resulted from replacement of the T-loop with the GAAA tetraloop.

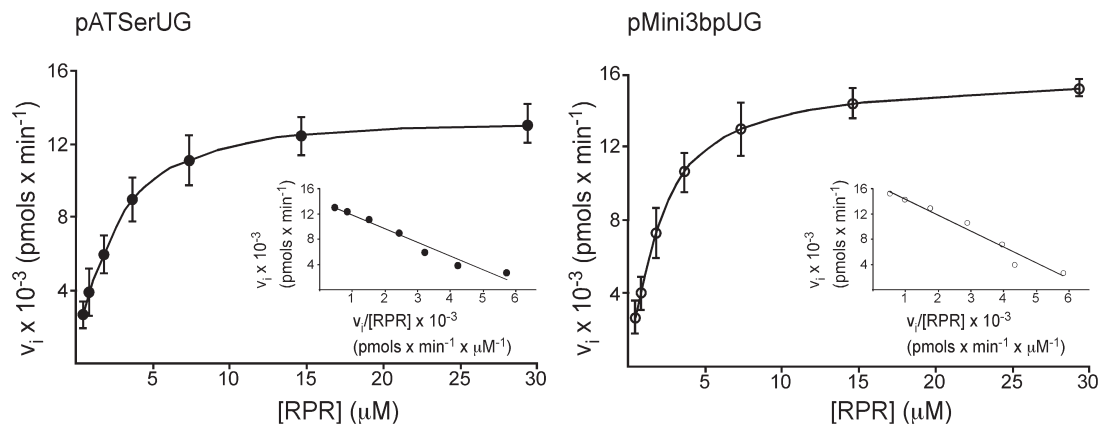


Figure 4. Rate of cleavage of pATSerUG and pMini3bpUG as a function of increasing concentration of *Pfu* RPR. Cleavage rate of pATSerUG and pMini3bpUG plotted as function of [*Pfu* RPR]. The experiment was conducted at 37°C in buffer C containing 800mM Mg²⁺ (see ‘Materials and Methods’ section). The data represent mean and experimental errors calculated from at least three independent experiments. Insets correspond to Eadie–Hofstee plots using the primary kinetic data. The k_{obs} and k_{obs}/K^{510} values are summarized in Table 1.

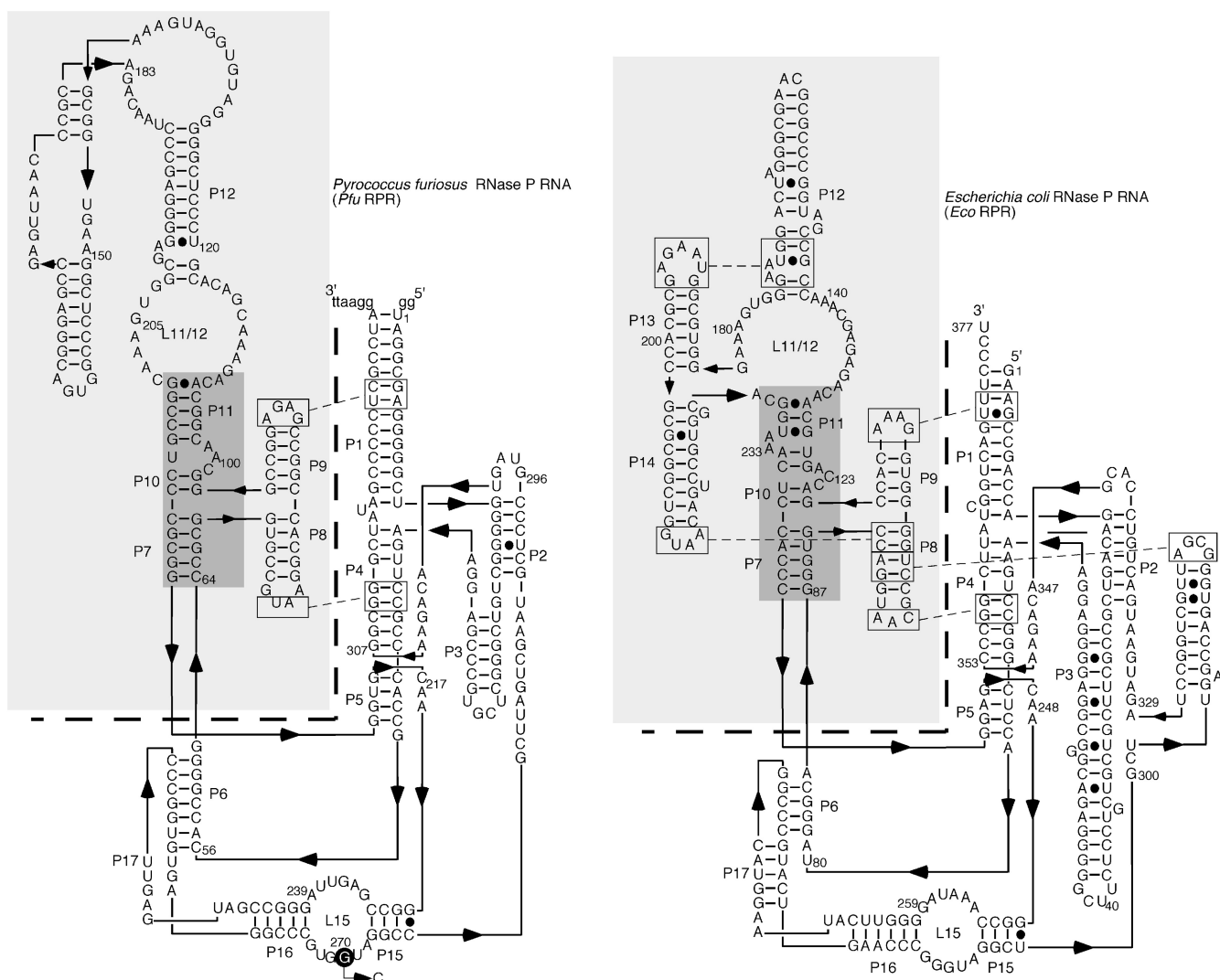


Figure 5. Illustrations of the predicted secondary structures of *Pfu* and *Eco* (M1 RNA) RPRs (6,50,54). The specificity (S) (highlighted in light grey) and catalytic (C) domains are as indicated and the P10–P11 regions in the respective RNA are highlighted in dark grey. The S domain (light grey) of *Pfu* RPR was replaced with that of *Eco* RPR and the corresponding mutant is referred to as *Pfu* RPR_{Ecs3} (for details, see text). The *Pfu* RPR_{C270} variant harbors a change in the GGU-motif in the P15-loop that interacts with the 3'-NCC in the substrate.

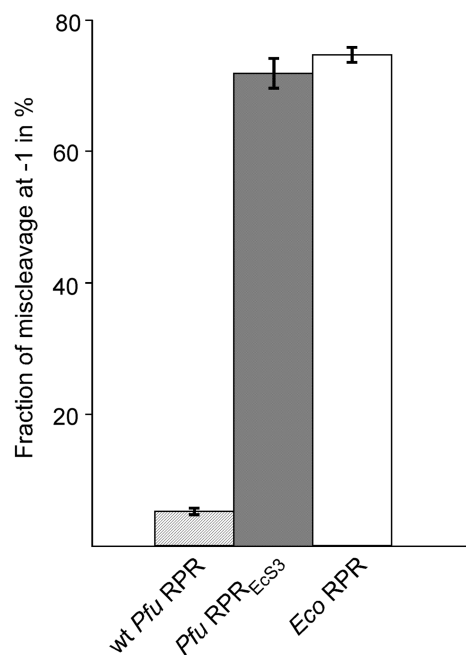


Figure 6. Frequency of mis-cleavage of pATSerCG_{GAAA} by wt *Pfu* RPR, *Pfu* RPR_{EcS3} and *Eco* RPR at the -1 position as indicated. The experiment was performed 37°C in buffer C containing 800 mM Mg²⁺. The final concentration of RPR was ~ 1.8 – 3.6 μ M (wt *Pfu* RPR), 4.9 μ M (*Pfu* RPR_{EcS3}) and 3.7 μ M (*Eco* RPR), while the substrate concentration was ~ 0.02 μ M. The incubation time for the reactions were 234–257 min (wt *Pfu* RPR and *Pfu* RPR_{EcS3}) and 0.5 min (*Eco* RPR).

Previous studies with the bacterial RPR concluded that miscleavage is linked to the presence of the C₋₁/G₊₇₃ pair in the substrate (34–40,43). Therefore, to understand whether cleavage of pATSerCG_{GAAA} at the -1 position depends on the identity of the residue at -1 and/or the C₋₁/G₊₇₃ pair, we analyzed the cleavage patterns of several pATSer derivatives, referred to as pATSerUA, pATSerCA, pATSerUA_{GAAA}, pATSerCA_{GAAA} and pATSerUG_{GAAA} (Figure 1). All these substrates were cleaved preferentially at $+1$ with and without the various combinations of the *Pfu* RPPs both at 30 and 300 mM Mg²⁺ (data only shown for pATSerUG_{GAAA}, Figure 7B). Therefore, we conclude that the C₋₁/G₊₇₃ base pair in pATSerCG_{GAAA} influences the cleavage-site selection process in the presence of RPP21•RPP29 and to a lesser extent in the presence of only POP5•RPP30.

Influence of POP5•RPP30 on cleavage-site recognition. As discussed above, hairpin loop substrates consisting of only 3 and 4-bp long stems (pMini3bpUG and pMini3bpCG) were cleaved in the presence of the different *Pfu* RPPs. The pMini3bp substrates most likely do not interact with the TBS-region of the RPR rather this type of substrates relies mainly on the interactions between RPR and the 3'-end as well as the residue at -1 of the substrate (2). Consistent with this expectation, substitution of G₂₇₀ with C₂₇₀ in *Pfu* RPR (*Pfu* RPR_{C270}) resulted in lower cleavage efficiency of pMini3bpCG as well as cleavage mainly at -1 . Conversely, changing C₊₇₄ (the first C at the 3'-end; Figure 1) to G₊₇₄ reduced the rate and resulted

in miscleavage at -1 by the wt *Pfu* RPR while *Pfu* RPR_{C270} cleaved this mutant substrate more like wt *Pfu* RPR [Figure 2 in Supplementary Data; see also (44)]. This result led us to postulate that cleavage of pMini3bp substrates might yield clues as to which of the two binary complexes might affect the interactions between the RPR and the -1 position and the 3'-end of the substrate.

Regardless of whether we used pMini3bpUG or pMini3bpCG, RPP21•RPP29 was unable to aid the *Pfu* RPR to cleave these substrates at 30 mM Mg²⁺. In stark contrast, both substrates were cleaved efficiently by *Pfu* RPR + POP5•RPP30 (Figure 7C and F), as expected from the ability of this binary complex to bind to the C domain (6,42) and thereby promote substrate interactions with the -1 position and/or the NCCA-motif at the 3'-end. However, there are some differences in the cleavage sites chosen. With pMini3bpUG, cleavage was mainly at $+1$ (Figure 7C, lane 4). In contrast, pMini3bpCG was cleaved at both $+1$ and -1 with approximately equal frequency (Figure 7F, lane 4). We also note that increasing the Mg²⁺ concentration resulted in a reduction in cleavage at the -1 position in the presence of POP5•RPP30. From these data, we conclude that the POP5•RPP30 protein complex influences cleavage-site selection for substrates with only the -1 and 3'-NCCA determinants present.

DISCUSSION

General framework for understanding substrate recognition by RNase P

To appreciate the similarities and differences in substrate recognition by archaeal and bacterial RNase P, we first elaborate a general working model for cleavage-site selection. Efficient cleavage at the correct position depends on the coordinated recognition of several determinants, whose hierarchy remains unclear. The TSL/TBS-, RCCA-RNase P RNA (interacting residues underlined), A₂₄₈/N₋₁ and G₊₁/unknown (RPR) motif interactions represent four different substrate–bacterial RPR interactions that are vital for (i) binding the substrate and positioning chemical groups at the site of cleavage, (ii) exposing the scissile linkage for nucleophilic attack, (iii) preventing a nucleophilic attack by the 2'-OH at position -1 (corresponds to a negative determinant) and (iv) positioning the catalytic metal ions, which promote the chemical cleavage (numbering of residues based on *Eco* RPR). Mutant bacterial RPRs or substrates in which these contacts were individually disrupted reveal some redundancy in the determinants required to specify the cleavage site. Moreover, several experimental observations support the idea that interactions between the RPR/RPPs and substrate influence both the positioning and affinity of the metal ions at the site of cleavage (2,3,45,46).

The bacterial RPR is made up of two independently folding modules termed the catalytic (C) and specificity (S) domains, with the former responsible for cleavage of the scissile linkage in the substrate [Figure 5; (47,48); see also (6)]. The S domain recognizes the TSL region in the pRNA, and this interaction is believed to promote an

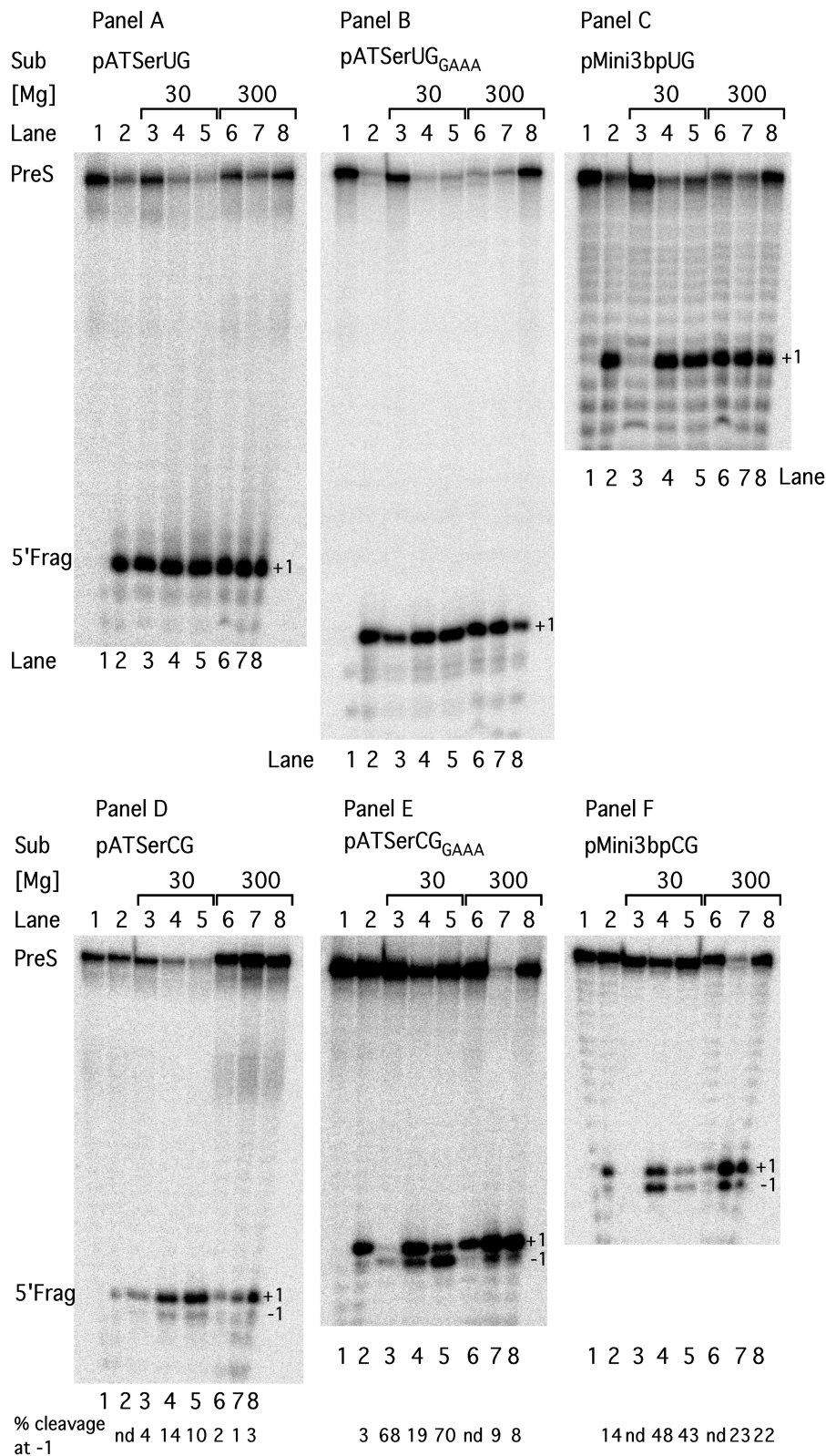


Figure 7. Cleavage of various model hairpin substrates by *Pfu* RPR with and without RPPs. Panels A–F show cleavage of pATSerUG, pATSerUG_{GAAA}, pMini3bpUG, pATSerCG, pATSerCG_{GAAA} and pMini3bpCG, respectively. The RPR-alone reactions were performed in buffer C containing 800 mM Mg²⁺, while those in the presence of RPPs were performed at 37°C in buffer D containing either 30 or 300 mM Mg²⁺ (as indicated). In each panel, the lanes correspond to: 1, no enzyme; 2, *Pfu* RPR alone; 3 and 6, *Pfu* RPR + RPP21•RPP29; lanes 4 and 7, *Pfu* RPR + POP5•RPP30 and lanes 5 and 8, *Pfu* RPR + all four proteins. %cleavage at –1, frequency of cleavage at this position; ND, not determined.

induced fit in the C domain that positions chemical groups and/or catalytically important Mg^{2+} near the correct cleavage, thus preventing miscleavage (28,39,40). If a correct 'TSL/TBS interaction' is established (e.g. in the case of pATSerUG), then chemical groups and/or Mg^{2+} at the cleavage site are organized to promote cleavage at +1. If this interaction is absent or altered, the cleavage at +1 could still be favored provided other determinants are in place (the A_{248}/N_{-1} and the $RCCA$ -RNase P interactions; e.g. the case with pATSerUG_{GAAA}). However, if the 'TSL/TBS interaction' is altered or missing along with one of these other determinants (e.g. pATSerCG_{GAAA} or pMini3bpCG), then miscleavage occurs at -1. This is likely due to a change in positioning of chemical groups and/or catalytic Mg^{2+} required for cleavage at +1. Alternatively, although not mutually exclusive, the inability to either disrupt the C_{-1}/G_{+73} pair in these substrates or promote formation of the ' A_{248}/N_{-1} interaction' could result in miscleavage at -1 (Figure 5).

Cleavage of model substrates by archaeal and bacterial RPRs: parallels and differences

Pfu RPR cleaves model hairpin loop substrates as demonstrated previously for both bacterial and eukaryal RNase P RNA (7,27). The rate of pATSerUG cleavage by *Pfu* RPR was 200-fold lower compared to that of *Eco* RPR (M1 RNA) under saturating Mg^{2+} -concentrations at pH 6.1 and 37°C; however, *Pfu* RPR, which functions in a hyper-thermophilic organism, predictably displayed a 65-fold higher rate at 55°C compared with 37°C (3.8 versus 0.058 min⁻¹; Table 1). This near coincidence of rates of pATSerUG cleavage by *Pfu* and *Eco* RPRs at 800 mM NH_4^+ and Mg^{2+} suggests that the archaeal RPR is catalytically as competent as its bacterial cousin in the presence of high concentrations of NH_4^+ and Mg^{2+} , reinforcing the idea of functional equivalence of the C domains of bacterial and archaeal RPRs, first deduced from sequence comparisons (49). However, this similarity could be uncovered only when structural defects in the archaeal RPR, due to the lack of stabilizing structural elements present in the bacterial RPR (45), are ameliorated by selected assay conditions. A recent study drew a similar inference, albeit the functional parallel became evident after introducing minimal changes in the archaeal RPR to mimic the bacterial counterpart (8). [Note: Based on structural variations, archaeal RPRs are classified into types A and M (49). Currently, our inferences apply to type A, of which *Pfu* RPR is a member.]

The near-similar rates of cleavage of a model substrate belie the different cleavage sites selected by *Eco* and *Pfu* RPRs. While *Eco* RPR cleaved pATSerCG_{GAAA} preferentially at -1, cleavage by *Pfu* RPR occurred mainly at +1 (Figure 1). Two reasons might account for the *Pfu* RPR's behavior. Although *Eco* and *Pfu* RPRs share universally conserved nucleotides and exhibit overall similarities in secondary structure (29,49,50), closer inspection reveals that their TBS regions are different (see P10-11 in Figure 5). There are two A-bulges in *Eco* RPR, while there is only one in *Pfu* RPR. We reason below why the altered TBS in the *Pfu* RPR might result in lack of

interactions with the T-loop in pATSerUG and the GAAA-tetraloop in pATSerCG_{GAAA}.

With *Eco* RPR, two observations support the idea that the TSL/TBS interaction influences events at the cleavage site. First, mutations in the P10-11 region of *Eco* RPR resulted in cleavage of pATSerCG_{GAAA} preferentially at the +1 (correct) site and suppression of miscleavage at -1 (28). Second, *Eco* RPR-mediated cleavage of pATSerUG and pMini3bpUG, which differ in the length of the acceptor- and T-stems equivalents, requires lower Mg^{2+} concentration for optimal cleavage of the former [(28), Wu *et al.*, manuscript in preparation]. In contrast, cleavage of these two substrates by *Pfu* RPR showed no difference in Mg^{2+} requirement (Figure 3); even their respective kinetic constants k_{obs} and k_{obs}/K^{sto} , K_d as well as the Hill coefficients for Mg^{2+} binding and K_d values are similar (Table 1). Moreover, replacing *Pfu* RPR's S domain with that of *Eco* RPR resulted in a chimeric RPR variant that cleaved pATSerCG_{GAAA} mainly at -1, which is nearly identical to how *Eco* RPR cleaves this substrate [Figures 3 and 6; (28)]. The longer stem and the presence of the T-loop in pATSerUG lowers the Mg^{2+} requirement for catalysis, probably due to the interactions that it promotes with the *Eco* RPR; the absence of such contacts with *Pfu* RPR might therefore account for the uniformly higher Mg^{2+} requirement to cleave both short- or long stem-containing model substrates.

While both the bacterial and archaeal RPRs cleave model substrates, there are clearly differences in how they recognize substrate structural elements. Recent data strongly support the premise that the structural differences in the TBS-region of *Eco* and *Pfu* RPRs might result in weaker/altered substrate recognition by the latter. Replacing the S domain of the archaeal *Methanothermobacter thermautotrophicus* (*Mth*) RPR with the corresponding S domain from *Eco* RPR improved the catalytic activity of the chimeric RPR, likely due to improved substrate binding conferred by the bacterial RPR's S domain (8). Moreover, covalent tethering of a ptRNA to *Methanocaldococcus jannaschii* (*Mja*) RPR resulted in accurate self-cleavage (0.05 min⁻¹ at pH 5.1) even though this archaeal RPR, under various conditions tested so far, is unable to cleave a ptRNA in trans (9). Since *Mja* RPR is missing both A-bulges in the TBS, efficient TSL recognition and ptRNA processing is unlikely.

Insights into the role of RPPs in substrate recognition and cleavage-site selection

Footprinting studies indicate that RPP21•RPP29 and POP5•RPP30 interact with the S and C domains, respectively (6,42). This demarcation is consistent with results from single-turnover kinetic studies, which indicate that POP5•RPP30 (but not RPP21•RPP29) is solely responsible for increasing the rate of the phosphodiester bond-breaking step [(9); Chen *et al.*, in press]. Conversely, RPP21•RPP29 (and not POP5•RPP30) lowers the apparent K_m indicating its role in increasing the RPR's affinity for ptRNA substrate (Chen *et al.*, in press). Although the two archaeal binary RPP complexes

fulfil different (if partly overlapping) roles by binding to distinct parts of the RPR, both appear capable of influencing cleavage-site selection, although through distinct mechanisms.

As discussed above, the archaeal RPR's S domain (unlike the bacterial RPR) appears incapable of recognizing the TSL region in the substrates. However, our data indicate that the binding of RPP21•RPP29 renders the archaeal RPR's S domain a mimic of the bacterial counterpart in terms of substrate recognition. Somehow, it mediates directly (or indirectly via the RPR) recognition of the substrate's TSL, a cleavage-site determinant. One would predict then that while the *Pfu* RPR would be indifferent to the presence of the T-loop in influencing cleavage-site selection, the RPR + RPP21•RPP29 complex (by virtue of its ability to recognize the T-loop) would be sensitive to the presence of a T-loop or a GAAA tetraloop and exhibit a shift in the cleavage site when the TSL/TBS interaction is altered. Indeed, while the *Pfu* RPR cleaved both pATSerCG and pATSerCG_{GAAA} preferentially at +1, the *Pfu* RPR + RPP21•RPP29 complex cleaved the former at +1 and the latter mainly at -1 (akin to *Eco* RPR; Figure 7E). However, note that the cleavage site also depends on the structural topography of the -1/+73 pair in the substrate, i.e. C₋₁/G₊₇₃ versus U₋₁/G₊₇₃ (Figure 7B and E). Together, these data suggest that binding of RPP21•RPP29 to the *Pfu* RPR results in convergence of the archaeal RPR's substrate-recognition properties with those of the bacterial RPR.

In bacterial RPRs, the GGU-motif in the P15-loop pairs with the 3' NCCA-motif in the substrate forming the 'RCCA-RNase P RNA interaction' [interacting residues underlined; (2,51–53)]. Although not comprehensively studied as in the bacterial context, this interaction has been suggested to be important for ptRNA processing by the *Pyrococcus horikoshii* RNase P holoenzyme (44). Based on compensatory mutations to rescue artificially engineered base-pairing defects, we have validated this interaction in the *Pfu* RPR-alone reaction (Figure 2 in Supplementary Data). Moreover, since POP5•RPP30 binds to the C domain near the P15-loop and there is evidence of crosstalk between metal ions at and in the vicinity of the RCCA-RNase P RNA interaction and those at the cleavage site during bacterial RNase P catalysis (6,31,39,40), we predict that POP5•RPP30 would influence the positioning of catalytic Mg²⁺ ions. In this context, when the TSL/TBS interaction is absent (e.g. in the case of pATSerCG_{GAAA}), POP5•RPP30 promotes cleavage mainly at +1 in contrast to cleavage preferentially at -1 observed with RPP21•RPP29 (Figure 7E, compare lanes 3 and 4). Extending these studies to all four RPPs yields an interesting insight regarding the possible hierarchy of ES interactions that likely dictate catalytic metal ion positioning and/ or affinity, and thereby cleavage-site selection. In the presence of all four RPPs, the RPR cleaves pATSerCG_{GAAA} largely at -1 (Figure 7E, lane 5). The TSL/TBS interaction (even if it deviates from the norm as in pATSerCG_{GAAA}) promoted by RPP21•RPP29 appears therefore to override the influence of POP5•RPP30 via the P15-loop in organizing

events at and in the vicinity of the cleavage site, including the catalytic metal ions.

Another inference emerges from comparing the *Pfu* RPR + POP5•RPP30-mediated cleavages of pATSerCG_{GAAA} (cleaved mainly at +1) and pMini3bpCG (cleaved ~50% at +1). In the latter instance, there are only two determinants: the -1 residue (the A₂₄₈/N₋₁ interaction) and the 3'-NCCA-motif. It appears that the absence of a long acceptor stem might result in the modestly decreased cleavage of pMini3bpCG at the -1 position. In the presence of all four RPPs, the cleavage of pMini3bpCG at +1 (~50%) parallels that observed with POP5•RPP30, as might be anticipated from the negligible or lack of contribution of RPP21•RPP29 for a substrate that lacks a T-loop capping the acceptor/T-stem (e.g. pATSerCG_{GAAA}). Thus, the functional interplay between the RPR/RPPs and substrate is clearly dependent on the structural features present in substrates.

CONCLUDING REMARK

The identification of small model substrates that are efficiently cleaved by *in vitro* assembled archaeal RNase P, coupled with the availability of facile methods to incorporate site-specific modifications during chemical synthesis of small RNAs, should motivate studies to elucidate structure-activity relationships in substrates and map the structural features in archaeal RNase P critical for substrate recognition.

SUPPLEMENTARY DATA

Supplementary Data are available at NAR Online

ACKNOWLEDGMENTS

We are grateful to the members of the Gopalan and Kirsebom laboratories for helpful assistance.

FUNDING

Swedish Research Council (to L.A.K.); Uppsala RNA Research Center (Linné support to L.A.K.); National Institutes of Health (RO1 GM067807 to Mark P. Foster and V.G.; R21 AI082242 to Daniel R. Schoenberg and V.G.); NSF (MCB 0843543 to V.G.). Funding for open access charge: Swedish Research Council.

Conflict of interest statement. None declared.

REFERENCES

- Gopalan, V. and Altman, S. (2006) In Gesteland, R.F., Cech, T.R. and Atkins, J.F. (eds), *The RNA World*, 3rd edn. Cold Spring Harbor Press, Cold Spring Harbor, NY, (<http://rna.cshl.edu>).
- Kirsebom, L.A. (2007) RNase P RNA mediated cleavage: Substrate recognition and catalysis. *Biochimie*, **89**, 1183–1194.
- Kirsebom, L.A. and Trobro, S. (2009) RNase P RNA-mediated cleavage. *IUBMB Life*, **61**, 189–200.
- Guerrier-Takada, C., Gardiner, K., Marsh, T., Pace, N. and Altman, S. (1983) The RNA moiety of ribonuclease P is the catalytic subunit of the enzyme. *Cell*, **35**, 849–857.

5. Pannucci, J.A., Haas, E.S., Hall, T.A. and Brown, J.W. (1999) RNase P RNAs from some archaea are catalytically active. *Proc. Natl Acad. Sci. USA*, **96**, 7803–7808.
6. Tsai, H.Y., Pulukkunat, D.K., Woznick, W.K. and Gopalan, V. (2006) Functional reconstitution and characterization of *Pyrococcus furiosus* RNase P. *Proc. Natl Acad. Sci. USA*, **103**, 16147–16152.
7. Kikovska, E., Svärd, S.G. and Kirsebom, L.A. (2007) Eukaryotic RNase P RNA mediates cleavage in the absence of protein. *Proc. Natl Acad. Sci. USA*, **104**, 2062–2067.
8. Li, D., Willkomm, D.K. and Hartmann, R.K. (2008) Minor changes largely restore catalytic activity or archaeal RNase P RNA from *Methanothermobacter thermoautotrophicus*. *Nucleic Acids Res.*, **37**, 231–242.
9. Pulukkunat, D.K. and Gopalan, V. (2008) Studies on *Methanocaldococcus jannaschii* RNase P reveal insights into the roles of RNA and protein cofactors in RNase P catalysis. *Nucleic Acids Res.*, **36**, 4172–4180.
10. Holzmann, J., Frank, P., Löffler, E., Bennett, K.L., Gerner, C. and Rossmann, W. (2008) RNase P without RNA: identification and functional reconstitution of the human mitochondrial tRNA processing enzyme. *Cell*, **135**, 462–474.
11. Tallsjö, A. and Kirsebom, L.A. (1993) Product release is a rate-limiting step during cleavage by the catalytic RNA subunit of *Escherichia coli* RNase P. *Nucleic Acids Res.*, **21**, 51–57.
12. Peck-Miller, K. and Altman, S. (1991) Kinetics of the processing of the precursor to 4.5 S RNA, a naturally occurring substrate for RNase P from *Escherichia coli*. *J. Mol. Biol.*, **221**, 1–5.
13. Liu, F. and Altman, S. (1994) Differential evolution of substrates for an RNA enzyme in the presence and absence of its protein cofactor. *Cell*, **77**, 1093–1100.
14. Park, B.H., Lee, J.H., Kim, M. and Lee, Y. (2000) Effects of C5 protein on *Escherichia coli* RNase P catalysis with a precursor tRNA^{Phe} bearing a single mismatch in the acceptor stem. *Biochem. Biophys. Res. Commun.*, **268**, 136–140.
15. Loria, A. and Pan, T. (2001) Modular construction for function of a ribonucleoprotein enzyme: the catalytic domain of *Bacillus subtilis* RNase P complexed with *B. subtilis* RNase P protein. *Nucleic Acids Res.*, **29**, 1892–1897.
16. Buck, A.H., Dalby, A.B., Poole, A.W., Kazantsev, A.V. and Pace, N.R. (2005) Protein activation of a ribozyme: the role of bacterial RNase P protein. *EMBO J.*, **24**, 3360–3368.
17. Buck, A.H., Kazantsev, A.V., Dalby, A.B. and Pace, N.R. (2005) Structural perspective on the activation of RNase P RNA by protein. *Nat. Struct. Mol. Biol.*, **12**, 958–964.
18. Cray, S.M., Niranjanakumari, S. and Fierke, C.A. (1998) The protein component of *Bacillus subtilis* ribonuclease P increases catalytic efficiency by enhancing interactions with the 5' leader sequence of pre-tRNA^{Asp}. *Biochemistry*, **37**, 9409–9416.
19. Sun, L., Campell, F.E., Zahler, N.H. and Harris, M.E. (2006) Evidence that substrate-specific effects of C5 protein lead to uniformity in binding and catalysis by RNase P. *EMBO J.*, **25**, 3998–4007.
20. Kurz, J.C. and Fierke, C.A. (2002) The affinity of magnesium binding sites in the *Bacillus subtilis* RNase P-pre-tRNA complex is enhanced by the protein subunit. *Biochemistry*, **41**, 9545–9548.
21. Sun, L. and Harris, M.E. (2007) Evidence that binding of C5 protein to P RNA enhances ribozyme catalysis by influencing active site metal ion affinity. *RNA*, **13**, 1505–1515.
22. Niranjanakumari, S., Stams, T., Cray, S.M., Christianson, D.W. and Fierke, C.A. (1998) Protein component of the ribozyme ribonuclease P alters substrate recognition by directly contacting precursor tRNA. *Proc. Natl Acad. Sci. USA*, **95**, 15212–15217.
23. Yuan, Y. and Altman, S. (1995) Substrate recognition by human RNase P: identification of small, model substrates for the enzyme. *EMBO J.*, **14**, 159–168.
24. Cooley, L., Appel, B. and Söll, D. (1982) Post-transcriptional nucleotide addition is responsible for the formation of the 5' terminus of histidine tRNA. *Proc. Natl Acad. Sci. USA*, **79**, 6475–6479.
25. Orellana, O., Cooley, L. and Söll, D. (1986) The additional guanylate at the 5' terminus of *Escherichia coli* tRNA^{His} is the result of unusual processing by RNase P. *Mol. Cell Biol.*, **6**, 525–529.
26. Carrara, G., Calandra, P., Fruscoloni, P., Doria, M. and Tocchini-Valentini, G.P. (1989) Site selection by *Xenopus laevis* RNase P. *Cell*, **58**, 37–45.
27. McClain, W.H., Guerrier-Takada, C. and Altman, S. (1987) Model substrates for an RNA enzyme. *Science*, **238**, 527–530.
28. Brännvall, M., Kikovska, E., Wu, S. and Kirsebom, L.A. (2007) Evidence for induced fit in bacterial RNase P RNA-mediated cleavage. *J. Mol. Biol.*, **372**, 1149–1164.
29. Gopalan, V. (2007) Uniformity amid diversity in RNase P. *Proc. Natl Acad. Sci. USA*, **104**, 2031–2302.
30. Milligan, J.F., Groebe, D.R., Withrell, G.W. and Uhlenbeck, O.C. (1987) Oligoribonucleotide synthesis using T7 RNA polymerase and synthetic DNA templates. *Nucleic Acids Res.*, **15**, 8783–8798.
31. Brännvall, M., Kikovska, E. and Kirsebom, L.A. (2004) Cross talk in RNase P RNA mediated cleavage. *Nucleic Acids Res.*, **32**, 5418–5429.
32. Stage-Zimmermann, T. and Uhlenbeck, O.C. (1998) Hammerhead ribozyme kinetics. *RNA*, **4**, 875–889.
33. Kurz, J. and Fierke, C.A. (2002) The affinity of magnesium binding sites in the *Bacillus subtilis* RNase P•Pre-tRNA complex is enhanced by the protein subunit. *Biochemistry*, **41**, 9545–9558.
34. Brännvall, M. and Kirsebom, L.A. (1999) Manganese ions induce miscleavage in the *Escherichia coli* RNase P RNA-catalyzed reaction. *J. Mol. Biol.*, **292**, 53–63.
35. Brännvall, M. and Kirsebom, L.A. (2001) Metal ion cooperativity in ribozyme cleavage of RNA. *Proc. Natl Acad. Sci. USA*, **98**, 12943–12947.
36. Brännvall, M. and Kirsebom, L.A. (2005) Complexity in orchestration of chemical groups near different cleavage sites in RNase P RNA mediated cleavage. *J. Mol. Biol.*, **351**, 251–257.
37. Brännvall, M., Pettersson, B.M.F. and Kirsebom, L.A. (2002) The residue immediately upstream of the RNase P cleavage site is a positive determinant. *Biochimie*, **84**, 693–703.
38. Brännvall, M., Pettersson, B.M.F. and Kirsebom, L.A. (2003) Importance of the +73/294 interaction in *Escherichia coli* RNase P RNA substrate complexes for cleavage and metal ion coordination. *J. Mol. Biol.*, **325**, 697–709.
39. Kikovska, E., Brännvall, M., Kufel, J. and Kirsebom, L.A. (2005) Substrate discrimination in RNase P RNA-mediated cleavage: importance of the structural environment of the RNase P cleavage site. *Nucleic Acids Res.*, **33**, 2012–2021.
40. Kikovska, E., Mikkelsen, N.-E. and Kirsebom, L.A. (2005) The naturally trans-acting ribozyme RNase P RNA has leadzyme properties. *Nucleic Acids Res.*, **33**, 6920–6930.
41. Hartmann, R.K. and Erdmann, V.A. (1991) Analysis of the gene encoding the RNA subunit of ribonuclease P from *T. thermophilus* HB8. *Nucl. Acids Res.*, **19**, 5957–5964.
42. Xu, Y., Amero, C.D., Pulukkunat, D.K., Gopalan, V. and Foster, M.P. (2009) Solution structure of an archaeal RNase P binary protein complex: Formation of the 30-kDa complex between *Pyrococcus furiosus* RPP21 and RPP29 is accompanied by coupled protein folding and highlights critical features for protein-protein and protein-RNA interactions. *J. Mol. Biol.*, **393**, 1043–1055.
43. Pettersson, B.M.F. and Kirsebom, L.A. (2008) The presence of a C-1/G+73 pair in a tRNA precursor influences processing and expression *in vivo*. *J. Mol. Biol.*, **381**, 1089–1097.
44. Terada, A., Yoshida, T. and Kimura, M. (2007) Identification of nucleotide residues essential for RNase P activity from the hyperthermophilic archaeon *Pyrococcus horikoshii* OT3. *Biosci. Biotechnol. Biochem.*, **71**, 1940–1945.
45. Lai, L.B., Vioque, A., Kirsebom, L.A. and Gopalan, V. (2010) Unexpected diversity of RNase P, an ancient tRNA processing enzyme: challenges and prospects. *FEBS Lett.*, **584**, 287–296.
46. McClain, W.H., Lai, L.B. and Gopalan, V. (2010) Trials, travails and triumphs: an account of RNA catalysis in RNase P. *J. Mol. Biol.*, **397**, 627–646.

47. Pan, T. (1995) Higher order folding and domain analysis of the ribozyme from *Bacillus subtilis* ribonuclease P. *Biochemistry*, **34**, 902–909.
48. Green, C.J., Rivera-León, R. and Vold, B.S. (1996) The catalytic core of RNase P. *Nucleic Acids Res.*, **24**, 1497–1503.
49. Harris, J.K., Haas, E.S., Williams, D., Frank, D.N. and Brown, J.W. (2001) New insight into RNase P RNA structure from comparative analysis of the archaeal RNA. *RNA*, **7**, 220–232.
50. Brown, J. (1999) The ribonuclease P database. *Nucleic Acids Res.*, **27**, 314.
51. Kirsebom, L.A. and Svärd, S.G. (1994) Base pairing between *Escherichia coli* RNase P RNA and its substrate. *EMBO J.*, **13**, 4870–4876.
52. Svärd, S.G., Kagardt, U. and Kirsebom, L.A. (1996) Phylogenetic comparative mutational analysis of the base-pairing between RNase P RNA and its substrate. *RNA*, **2**, 463–472.
53. Kufel, J. and Kirsebom, L.A. (1996) Different cleavage sites are aligned differently in the active site of M1 RNA, the catalytic subunit of *Escherichia coli* RNase P. *Proc. Natl Acad. Sci. USA*, **93**, 6085–6090.
54. Massire, C., Jaeger, L. and Westhof, E. (1998) Derivation of the three-dimensional architecture of bacterial ribonuclease P RNAs from comparative sequence analysis. *J. Mol. Biol.*, **279**, 773–793.